*36th EPS Conference on Plasma Phys. Sofia, June 29 - July 3, 2009 ECA Vol.**33E**, P-1.131 (2009)*

Radial structure of the two magnetohydrodynamic GAMs existing in toroidally rotating tokamak plasmas

C. Wahlberg

Department of Physics and Astronomy, EURATOM/VR Fusion Association, P.O. Box 516, Uppsala University, SE-751 20 Uppsala, Sweden

The geodesic acoustic mode (GAM) and its low-frequency cousin, the zonal flow (ZF) eigenmode, are both presently of very large interest in tokamak physics. As recently shown in [1-3], toroidal plasma rotation increases the frequency of the GAM and also induces a finite eigenfrequency of the ZF eigenmode. Here, these two eigenfrequencies will be denoted by ω^2_{GAM1} (upper frequency) and ω^2_{GAM2} (lower frequency) and they are, for slow plasma rotation ($M_s << 1$, where M_s is the sonic Mach number), given by

$$\omega^2_{GAM1} = \omega_s^2\left(2+\frac{1}{q^2}+\frac{8M_s^2}{\Gamma}+...\right), \quad \omega^2_{GAM2} = \frac{M_s^2\Omega^2}{1+2q^2}\left(1-\frac{1}{\Gamma}\right)+... \ , \tag{1a, b}$$

where $\omega_s \equiv v_s / R_0$ is the sound frequency, Ω the toroidal rotation frequency at the flux surface with safety factor q, and Γ is the adiabatic index. The expressions above are valid for the axisymmetric ($m = n = 0$) form of the modes [1-3]. For non-axisymmetric GAMs, having the form of continuum modes with finite m and n at the resonant surface $q = m/n$, Eqs. (1a, b) denote the Doppler-shifted eigenfrequencies $(\omega + n\Omega)^2$ [1, 3, 4].

In the present work, the radial structure of both of the axisymmetric GAMs above in a rotating plasma are calculated within the linear, ideal MHD model [3], starting from the Frieman-Rotenberg MHD stability equation for a Lagrangian perturbation $\boldsymbol{\xi} \sim e^{-i\omega t}$ in a plasma with stationary mass flow:

$$\rho\omega^2\boldsymbol{\xi} + 2i\rho\omega\mathbf{v}\cdot\nabla\boldsymbol{\xi} - \rho\mathbf{v}\cdot\nabla\left[(\mathbf{v}\cdot\nabla)\boldsymbol{\xi}\right] + \nabla\cdot\left[\rho\boldsymbol{\xi}(\mathbf{v}\cdot\nabla)\mathbf{v}\right] + \mathbf{F}(\boldsymbol{\xi},\mathbf{Q}) = 0\,, \tag{2}$$

where $\mathbf{Q} = \nabla\times(\boldsymbol{\xi}\times\mathbf{B})$ is the perturbed magnetic field, $\mathbf{v}$ the equilibrium flow velocity, $\mathbf{B}$ the equilibrium magnetic field, $\mathbf{F}(\boldsymbol{\xi},\mathbf{Q}) = -\nabla\delta P + \left[(\mathbf{B}\cdot\nabla)\mathbf{Q} + (\mathbf{B}\cdot\nabla)\mathbf{Q}\right]/\mu_0$ the force operator, $\delta P = -\boldsymbol{\xi}\cdot\nabla p - \Gamma p\nabla\cdot\boldsymbol{\xi} + \mathbf{B}\cdot\mathbf{Q}/\mu_0$ the perturbed, total pressure, and p denotes the equilibrium plasma pressure. Here, we represent $\boldsymbol{\xi}$ and $\mathbf{Q}$ by their contravariant components, i.e. $\boldsymbol{\xi} = \xi^r\mathbf{e}_r + \xi^\theta\mathbf{e}_\theta + \xi^\varphi\mathbf{e}_\varphi$ and $\mathbf{Q} = Q^r\mathbf{e}_r + Q^\theta\mathbf{e}_\theta + Q^\varphi\mathbf{e}_\varphi$, where $\mathbf{e}_r$, $\mathbf{e}_\theta$ and $\mathbf{e}_\varphi$ are the covariant basis vectors of the flux coordinates (r, θ, φ). Furthermore, we make the following perturbation expansion of these components of $\boldsymbol{\xi}$ and $\mathbf{Q}$:

$$\xi^r = \varepsilon^2\left(\xi_2^{r(2)}e^{2i\theta} + \xi_{-2}^{r(2)}e^{-2i\theta}\right) + \ldots\,, \tag{3a}$$

$$\xi^\theta = \xi_0^{\theta(0)} + \varepsilon\left(\xi_1^{\theta(1)}e^{i\theta} + \xi_{-1}^{\theta(1)}e^{-i\theta}\right) + \varepsilon^2\left(\xi_0^{\theta(2)} + \xi_2^{\theta(2)}e^{2i\theta} + \xi_{-2}^{\theta(2)}e^{-2i\theta}\right) + \ldots\,, \tag{3b}$$

$$\xi^\varphi = \varepsilon\left(\xi_1^{\varphi(1)}e^{i\theta} + \xi_{-1}^{\varphi(1)}e^{-i\theta}\right) + \varepsilon^2\left(\xi_0^{\varphi(2)} + \xi_2^{\varphi(2)}e^{2i\theta} + \xi_{-2}^{\varphi(2)}e^{-2i\theta}\right) + \ldots\,, \tag{3c}$$

$$Q^r = \varepsilon^3\left(Q_2^{r(3)}e^{2i\theta} + Q_{-2}^{r(3)}e^{-2i\theta}\right) + \ldots\,, \tag{3d}$$

$$Q^\theta = \varepsilon^3\left(Q_2^{\theta(3)}e^{2i\theta} + Q_{-2}^{\theta(3)}e^{-2i\theta}\right) + \ldots\,, \tag{3e}$$

$$Q^\varphi = \varepsilon^4\left(Q_1^{\varphi(4)}e^{i\theta} + Q_{-1}^{\varphi(4)}e^{-i\theta}\right) + \varepsilon^5\left(Q_0^{\varphi(5)} + Q_2^{\varphi(5)}e^{2i\theta} + Q_{-2}^{\varphi(5)}e^{-2i\theta}\right) + \ldots\,. \tag{3f}$$

The symbol ε and superscripts above denote the ordering with respect to the inverse aspect ratio of the plasma torus ($\varepsilon = r/R$). As seen in Eq. (3b) the eigenmode has, to leading order, the character of a "zonal flow" type of displacement $\xi_0^{\theta(0)}(r)$ on the magnetic surfaces, and it can be shown from Eq. (2) that $\xi_0^{\theta(0)}(r) = \hat{\xi}\delta(r - r_0)$, where $\hat{\xi}$ is an arbitrary amplitude constant and r_0 denotes a magnetic surface where $\omega^2 = \omega_{GAM1}^2$ or $\omega^2 = \omega_{GAM2}^2$ [3]. The other, leading-order components of the eigenmode consist of $Q_{\pm1}^{\varphi(4)}$, $\xi_{\pm1}^{\varphi(1)}$ and $\xi_{\pm1}^{\theta(1)}$, all localized on $r = r_0$, with the latter two quantities given by

$$\xi_{\pm1}^{\varphi(1)} = -\frac{r}{qR_0}\frac{\omega_s^2 + \Omega^2/2 \pm q\omega\Omega}{\left(\omega_s^2/q^2 - \omega^2\right)}\xi_0^{\theta(0)}\,, \tag{4}$$

and $\xi_{\pm1}^{\theta(1)} = \xi_{\pm1}^{\varphi(1)}/q$, respectively. Note the asymmetry of the $m = \pm1$ side-bands induced by the Coriolis force of the rotation, a phenomenon possibly useful as a diagnostic of plasma rotation [3].

To next order in epsilon, the toroidal $m = 0$ components $\xi_0^{\varphi(2)}$ and $Q_0^{\varphi(5)}$ in Eq. (3) are also localized on $r = r_0$, and expressions for these quantities can be found in [3]. To the same order, the solution in addition includes poloidal side-bands involving all $m = \pm2$ components of $\boldsymbol{\xi}$ and $\mathbf{Q}$ in Eq. (3), and existing outside the flux surface $r = r_0$. The radial structure of this surrounding "halo" is governed by the equation [3]

$$\frac{d}{dr}\left(\frac{r^3}{q^2}\frac{d\xi_{\pm2}}{dr}\right) - \frac{3r\xi_{\pm2}}{q^2} \pm \frac{r^3}{2}\frac{d}{dr}\left[Z_\pm(r)\delta(r - r_0)\right] = 0\,, \tag{5}$$

with $\xi_{\pm2}^{r(2)} = i\hat{\xi}\xi_{\pm2}$ and $Q_{\pm2}^{r(3)} = \pm 2iB_0\xi_{\pm2}^{r(2)}/R_0$. Furthermore,

$$Z_{\pm}(r) = \frac{\omega_s^2 + \Omega^2\left(1 + M_s^2/2\right)}{\omega_A^2} - \frac{\left(\omega_s^2 + \Omega^2/2 \pm q\omega\Omega\right)^2}{\omega_A^2\left(\omega_s^2 - q^2\omega^2\right)}, \tag{6}$$

where $\omega_A \equiv v_A / R_0$ denotes the Alfvén frequency. It follows from Eq. (5) that both $\xi_{\pm 2}$ and $\xi'_{\pm 2}$ will have discontinuities across $r = r_0$. These jumps in $\xi_{\pm 2}$ and $\xi'_{\pm 2}$ are easily shown to be given by $\left[\xi_{\pm 2}\right] = \mp\, q^2(r_0) Z_{\pm}(r_0)/2$ and $\left[\xi'_{\pm 2}\right] = \pm\, 3q^2(r_0) Z_{\pm}(r_0)/2r_0$, respectively [3]. Solutions of Eq. (5) exhibiting this property, using two different *q*-profiles, are shown in Figs. 1 and 2. In these figures, the symmetric ($\xi^s = \xi_{+2} + \xi_{-2}$) and antisymmetric ($\xi^a = \xi_{+2} - \xi_{-2}$) parts of the *r*-component of ξ in Eq. (3a) are shown.

Apart from a quadratic dependence on $q(r_0)$, coming from the jump conditions above, the single most important plasma parameter determining the $m = \pm 2$ amplitudes is the local beta value, via $Z_{\pm}(r_0)$ and $\omega_s^2/\omega_A^2 = \Gamma\beta(r_0)/2$. In both figures $\beta(r_0)$ = 0.02 has been used. Furthermore, the symmetric and antisymmetric amplitudes are plotted for the rotation frequencies Ω/ω_A = 0, 0.02, 0.04 in Figs. 1a and 2a, and for Ω/ω_A = 0.02, 0.04, 0.06 in Figs. 1b and 2b. In Fig. 1 the *q*-profile $q(r) = 1 + 3(r/a)^4$, with $q_a = 4$ and $r_0 = 0.7a$, has been used whereas $q(r) = 1 + 7(r/a)^{10}$, $q_a = 8$ and $r_0 = 0.5a$ in Fig. 2. In Figs. 1a and 2a, showing the radial structure of a GAM at the upper GAM frequency in Eq. (1a), only the antisymmetric part is finite in a nonrotating plasma. Furthermore, the amplitude is almost an order of magnitude larger in the outer region $r > r_0$ as compared with the amplitude in the inner region $r < r_0$, similar to the properties of the "global GAM" calculated numerically in [5]. With finite rotation, a symmetric part of ξ is also present and, at the largest rotation frequency in these figures, $\Omega/\omega_A = 0.04$, its amplitude is only around a factor of four smaller than the antisymmetric amplitude. In Figs. 1b and 2b, similar plots are shown for the GAM at the lower frequency, Eq. (1b). Here, the symmetric part is dominating and the amplitude of this part is, for the range of rotation frequencies shown, about an order of magnitude smaller than the antisymmetric amplitude of the mode at the higher GAM frequency.

References

[1] C. Wahlberg, Phys. Rev. Lett. **101**, 115003 (2008)

[2] S. Wang, Phys. Rev. Lett. **97**, 085002 (2006), Erratum **97**, 129902 (2006)

[3] C. Wahlberg, Plasma Phys. Controlled Fusion (accepted for publication)

[4] B. van der Holst B, A. J. C. Belien and J. P. Goedbloed, Phys. Plasmas **7**, 4208 (2000)

[5] H. L. Berk, C. J. Boswell, D. Borba, A. C. A. Figueiredo, T. Johnson, M. F. F. Nave, S. D. Pinches, S. E. Sharapov and JET EFDA contributors, Nucl. Fusion **46**, S888 (2006)

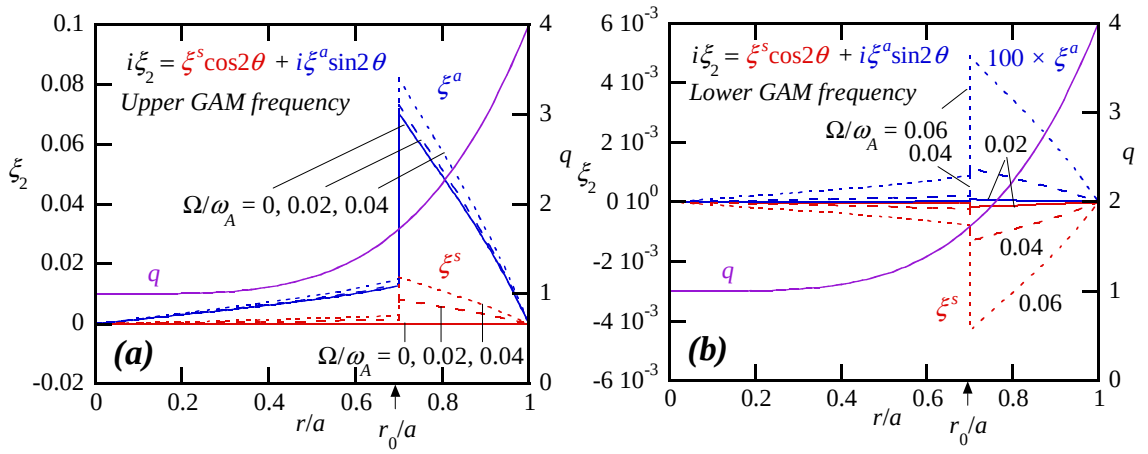

Figure 1. Amplitude of the symmetric and antisymmetric parts of the m = 2 side-band driven by a GAM localized at r/a = 0.7. The plasma has the q-profile $q(r) = 1 + 3(r/a)^4$ and the m = 2 amplitudes are shown for a few different Ω/ω_A. ***(a)*** Corresponds to a GAM at the upper (i.e. ordinary) GAM frequency, given by equation (1a), whereas ***(b)*** shows the corresponding amplitudes at the lower (i.e. ZF) GAM frequency, equation (1b).

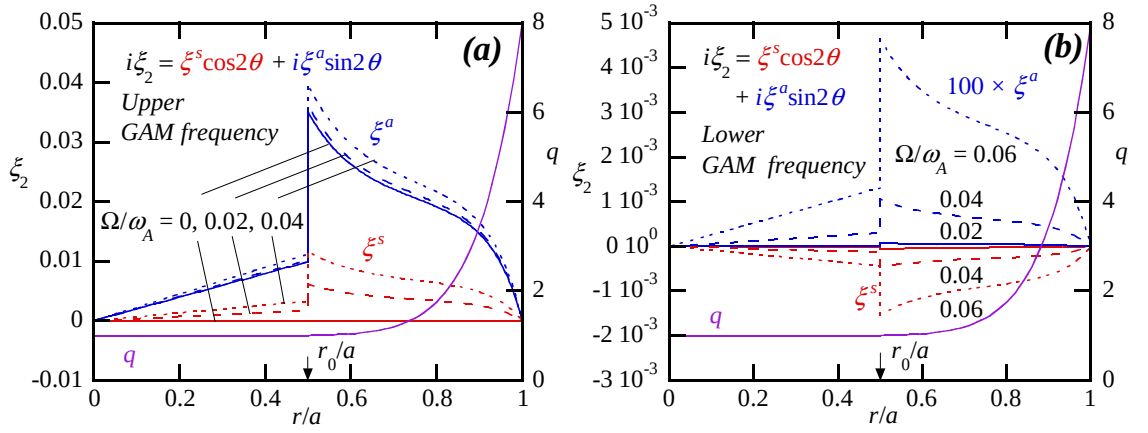

Figure 2. Amplitude of the symmetric and antisymmetric parts of the m = 2 side-band driven by a GAM localized at r/a = 0.5. The plasma has the q-profile $q(r) = 1 + 7(r/a)^{10}$ and the m = 2 amplitudes are shown for a few different Ω/ω_A. ***(a)*** Corresponds to a GAM at the upper (i.e. ordinary) GAM frequency, given by equation (1a), whereas ***(b)*** shows the corresponding amplitudes at the lower (i.e. ZF) GAM frequency, equation (1b).